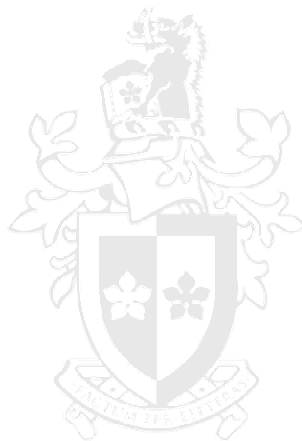


CFD Investigation for Turbidity Spikes in Drinking Water Distribution Networks

Alamgir Hossain

A thesis submitted to the
Faculty of Engineering and Industrial Sciences,
Swinburne University of Technology, Australia,
in fulfillment of the requirements for the degree of
Doctor of Philosophy.



August 2005

To my sister Late Rehena Khatun

Abstract

Drinking water distribution networks such as South East Water Ltd. (SEWL), Melbourne Water, Sydney Water, etc. are supposed to transport only dissolved matter rather than a few visible particles. However, it is almost impossible to make the drinking water free from suspended solid particles. The ability to determine the origins of these particles varies between different water supply systems, with possible sources being from catchment, treatment processes, biofilm growth within the water supply pipes, and corrosion products. Improvement of our understanding of the complex hydrodynamic behavior of suspended and/or deposited particles involved in these distribution pipe networks requires mathematical and physical models. Computational Fluid Dynamics (CFD) along with analytical turbulent model is one of the most popular mathematical techniques, which has the ability to predict the behavior of complex flows for such multiphase flow applications.

This study has been completed mainly in two steps. A CFD investigation was carried out to predict the hydrodynamic behavior of turbid particle flowing through a horizontal pipe networks including loop consist of bends and straight pipes. Furthermore, an extended analytical model was re-developed for the liquid-solid system to look at the similar behavior of the solid particles flowing in a turbulent field. These two parallel studies will provide better understandings about the turbidity spikes movements in the distribution networks.

A comprehensive CFD investigation was carried out for particle deposition in a horizontal pipe loop consisting of four 90° bends in a turbulent flow field. A satisfactory agreement was established with the experimental data as validation. This was a steady state multi-particle problem, which helped to understand the deposition characteristics for different particle sizes and densities at upstream and downstream sides of the bends as well as its circumference. Particle concentration was seen high at the bottom wall in the pipe flow before entering the bends, but for the downstream of bend the deposition was not seen high at the bottom as seen in upstream of bend rather inner side of the bend wall (60° skewed from bottom). The larger particles clearly showed deposition near the bottom of the wall except downstream. As expected, the smaller particles showed less tendency of deposition and this was more pronounced at higher velocity. Due to the high stream line curvature and associated centrifugal force acting on the fluid at different depths the particles became well mixed and resulted in homogeneous distribution near the bend regions.

The hydrodynamic behavior of particles flowing in a turbulent unsteady state flowing through a horizontal pipe was also studied to compare with the drinking water distribution networks data. In this numerical simulation six different flow-profiles and particle-load profiles were used to compute particles deposition and re-entrainment into the systems and to identify the conditions of the deposition and suspension mechanisms. Results showed that after a certain length of pipe and period of time after downward velocity gradient, when the velocity was constants over time, the shear stress was sufficiently high enough to cause the particle deposition on and roll along the bottom wall of pipe wall and created a secondary group of particle peak (called *kink*).

Finally, an extended analytical Turbulent Diffusion Model for liquid-solid phase was developed following an existing gas-liquid turbulence model. This turbulent diffusion model was then compared with the results of the CFD investigation making use of the same boundary conditions. The comparison established good agreement between these two models. The influence of velocity on the particle size distribution was dominant over the influence of the superficial liquid velocity, which was also explained by using the new parameter, velocity ratio. This velocity ratio was defined as the ratio between the free flight and gravitational velocity. Due to some inevitable assumptions used in the analytical model, the results showed typically less deposition as compared with the CFD investigation.

Acknowledgements

The author would like to acknowledge the supportive efforts of the many people and organizations that contributed to this research.

Dr. Jamal Naser, my supervisor, whose knowledge, patient teaching, and subtle direction guided me through this project and provided me with a great introduction into the field of research. I would like to thank him for such constant supervision in on and off campus.

I would like to acknowledge the South East Water Ltd., who provided the partial financial support to undertake this project. I would like to thank CSIRO for supporting and making the experimental data available to me, without that I could not authenticate my work. Clive Grainger, team leader of the experiment, CSIRO, is also deeply acknowledged for his important advices and support.

My beloved Mum and Dad, you were always encouraging and guiding me while I was away from you, which drove me forward. My sisters, brothers, and sister-in-laws, your inspirations helped me to endure the long journey.

All my friends inside and outside of the university, who I don't know they helped and inspired me, but they did.

Alamgir Hossain

Declaration of Originality

This thesis contains no material, which has been accepted for the award of any other degree in any university or institute of education; nor, to my best knowledge, does it contain material previously published by any other person, except where due reference is made in the body of the thesis.

Signed _____

[Alamgir Hossain]

Contents

	Page
Abstract	iii
Acknowledgements	vi
Declaration of Originality	vii
Contents	viii
List of Figures	xiii
List of Tables	xx
Chapter 1: Introduction	1-5
1.1 Background	1
1.2 Numerical Investigation	2
1.3 Analytical Model	2
1.4 The Objectives Of This Research.....	3
1.5 Thesis Outline.....	4
Chapter 1: Literature Review	6-22
2.1 Introduction	6
2.1.1 Methods of Investigation	7
Experimental investigation.....	8
Theoretical Calculation	8
Advantages of a Theoretical Calculation.....	9
Disadvantages of a Theoretical Calculation.....	10
Choice of Investigation in this Research.....	11
2.2 Particle Deposition in a Pipe Loop.....	12
2.3 Turbidity Spikes Movement.....	14
2.4 Particle Dispersion and Deposition Model	17
2.5 Numerical Simulation.....	20
2.6 Conclusion	22

Chapter 3: Governing Equations and Numerical Method	23-71
3.1 Introduction	23
3.2 Continuity and Momentum Equations	25
3.2.1 Definition of a Differential Equation	25
3.2.2 The General Differential Equation.....	27
3.2.3 The Mass Conservation Equation.....	28
3.2.4 Momentum Conservation Equations.....	28
3.3 Modelling Multiphase Flows	29
3.3.1 Multiphase Flow Regimes	29
Gas-liquid or liquid-liquid flows	30
Gas-solid flows	30
Liquid-solid flows	31
3.3.2 Examples of Multiphase Systems	31
3.3.3 Approaches to Multiphase Modelling	32
The Euler-Lagrange Approach.....	32
The Euler-Euler Approach	33
The VOF Model	35
The Mixture Model	35
The Eulerian Model	35
3.3.4 Choosing a Multiphase Model.....	36
Detailed Guidelines	37
The Effect of Particulate Loading	37
The Significance of the Stokes Number	38
3.4 The Multiphase Mixture Model	41
3.4.1 Overview of the Mixture Model	41
3.4.2 Limitations of the Mixture Model	41
3.4.3 Continuity Equation for the Mixture	42
3.4.4 Momentum Equation for the Mixture.....	43
3.4.5 Relative (Slip) Velocity and the Drift Velocity	43
3.4.6 Volume Fraction Equation for the Secondary Phases	45
3.5 Turbulent Modelling	45
3.5.1 Turbulence Model Selection for this Research.....	46
Reynolds-Averaged Approach vs. LES	46

Reynolds (Ensemble) Averaging	48
Boussinesq Approach vs. Reynolds Stress Transport Models	49
3.5.2 The Spalart-Allmaras Model	49
3.5.3 The Standard k- ϵ Model	50
3.5.4 The Standard k- ω Model	51
3.5.5 The Reynolds Stress Model (RSM)	51
3.5.6 Computational Effort: CPU Time and Solution Behavior	52
3.6 The Spalart-Allmaras Model	53
3.6.1 Transport Equation for the Spalart-Allmaras Model	53
3.6.2 Modelling the Turbulent Viscosity	54
3.6.3 Modelling the Turbulent Production	54
3.6.4 Modelling the Turbulent Destruction	56
3.6.5 Model Constants	56
3.6.6 Wall Boundary Conditions	57
3.7 Turbulent Boundary Conditions	57
3.7.1 Flow Inlets and Exits	57
Using Flow Boundary Conditions	57
Determining Turbulence Parameters	59
3.7.2 Uniform Specification of Turbulence Quantities	60
Turbulence Intensity	61
Turbulence Length Scale and Hydraulic Diameter	61
Turbulent Viscosity Ratio	62
3.7.3 Relationships for Deriving Turbulence Quantities	63
Estimating Modified Turbulent Viscosity from Turbulence Intensity and Length Scale	63
3.8 Numerical Simulation and Geometry Construction	63
3.8.1 Commercial Software	63
3.8.2 The Grid Topology	64
Choosing the Appropriate Grid Type	65
Setup Time	65
Computational Expense	66
Numerical Diffusion	66
3.8.3 Grid Requirements and Considerations	67
Geometry or Grid Requirements	68

Mesh Quality	68
Node Density and Clustering	68
Smoothness	70
Cell Shape	70
Flow-Field Dependency	70
3.9 Conclusion	71
Chapter 4: Particle Deposition in a Pipe Loop	72-93
4.1 Introduction	72
4.2 Numerical Technique	74
4.3 Result and Discussion	75
4.3.1 Model Validation	75
4.3.2 Particle Concentration at Different Depths across the Pipe	78
4.3.3 Circumferential Particle Deposition at Bends	83
4.3.4 Circumferential deposition at 3 rd bend	87
4.4 Conclusion	93
Chapter 5: Turbidity Spikes Movement	94-118
5.1 Introduction	94
5.2 Background	95
5.2.1 Definition of Turbidity	96
5.2.2 Formation of a Turbidity Spike	96
5.3 Numerical Simulation of Turbidity Spikes	99
5.3.1 Online Monitoring Data	99
5.3.2 Velocity and Particle-Load Profiles	101
5.3.3 Geometry and Boundary Conditions	104
5.4 Results and Discussion	105
5.4.1 Average Particle Distribution along the Pipe	105
5.4.2 Average Particle Deposition at Different Cross-sections	111
5.4.3 Gravity Deposition and Kink Formation	115
Kink Formation	116
5.5 Conclusion	117
Chapter 6: Turbulent Diffusion and Dispersion Model	119-196

6.1 Introduction	119
6.2 Analytical Turbulent Diffusion Model	122
6.2.1 Definition of the turbulent diffusion problem.....	127
6.2.2 Mathematical formulation of the model	131
6.3 Analytical Solution of the Problem.....	140
6.3.1 One Dimensional Problem	140
6.3.2 Extension to a two-dimensional deposition flux comparison with a semi empirical correlation	146
6.4 Cfd Investigation and Results Comparison	150
6.4.1 Relative Concentration along Height	150
6.4.2 Circumferential Deposition for the CFD Simulation.....	154
6.5 Conclusion	157
Chapter 7: Conclusion and Recommendations	160-162
7.1 Conclusion	160
7.2 Recommendations	162
Chapter 8: References	162-
	170
List of Personal Publications	171

List of Figures

	Page
Figure 3-1: Flux balance over a control volume.	26
Figure 3-2: Multiphase flow regimes.	30
Figure 4-1c: Schematic diagram of the pipe loop with four 90° bends.	73
Figure 4-2: Comparison of CFD results and experimental data (Grainger et al. 2003) for the velocity 0.4 ms^{-1} at center of the pipe (D is the diameter of pipe).	75
Figure 4-3: Comparison of CFD results and experimental data (Grainger et al. 2003) for different velocities at center of the pipe.	77
Figure 4-4: Contour of volume fraction of total particles at different heights (a, b, c, d, e, and f are for at 1, 5, 10, 20, 30, and 50 μm measured from bottom, respectively) for the velocity of 0.05 ms^{-1}	79
Figure 4-5: Velocity vector on a plane at different heights (a, b, c, and d are at 5, 10, 30, and 50 μm measured from bottom, respectively) at velocity 0.05 ms^{-1}	80
Figure 4-6: Velocity vector on a plane at different heights (a, b, c, and d are at 5, 10, 30, and 50 μm measured from bottom, respectively) at velocity 0.4 ms^{-1}	80-81
Figure 4-7: CFD investigation of particle concentration as function of velocity at different heights across the pipe at the measuring plane. ...	81
Figure 4-8a: Relative concentration of particles for different depths along the pipe at 0.05 ms^{-1}	82
Figure 4-8b: Relative concentration of particles for different depths along the pipe at 0.4 ms^{-1}	83

Figure 4-9: Vertical cross-section of a pipe.	83
Figure 4-10a: Cumulative particle deposition as a function of circumferential pipe angles at three different up and down stream of bends at 0.05 ms^{-1}	84
Figure 4-10b: Cumulative particle deposition as a function of circumferential pipe angles at three different up and down stream of bends at 0.1 ms^{-1}	84
Figure 4-10c: Cumulative particle deposition as a function of circumferential pipe angles at three different up and down stream of bends at 0.2 ms^{-1}	84
Figure 4-10d: Cumulative particle deposition as a function of circumferential pipe angles at three different up and down stream of bends at 0.3 ms^{-1}	85
Figure 4-10e: Cumulative particle deposition (CFD) as a function of circumferential pipe angles at three different up and down stream of bends at 0.4 ms^{-1}	85
Figure 4-11: Schematic diagram of a bend.....	87
Figure 4-12: Contour plot of particle volume fraction on three different cross-sectional planes for the velocity of 0.05, 0.1, 0.2, 0.3, and 0.4 ms^{-1} respectively.	88
Figure 4-13a: Particle deposition as a function of circumferential pipe angles θ at different planes of 3 rd bend at 0.05 ms^{-1}	89
Figure 4-13b: Particle deposition as a function of circumferential pipe angles θ at different planes of 3 rd bend at 0.1 ms^{-1}	89
Figure 4-13c: Particle deposition as a function of circumferential pipe angles θ at different planes of 3 rd bend at 0.2 ms^{-1}	89
Figure 4-13d: Particle deposition as a function of circumferential pipe angles θ at different planes of 3 rd bend at 0.3 ms^{-1}	90
Figure 4-13e: Particle deposition as a function of circumferential pipe angles θ at different planes of 3 rd bend at 0.4 ms^{-1}	90

Figure 4-14a: Particle deposition (CFD) as a function of circumferential pipe angles at the up and down stream of 3 rd bend for different particles at 0.05 ms ⁻¹	91
Figure 4-14b: Particle deposition (CFD) as a function of circumferential pipe angles at the up and down stream of 3 rd bend for different particles at 0.1 ms ⁻¹	92
Figure 4-14c: Particle deposition (CFD) as a function of circumferential pipe angles at the up and down stream of 3 rd bend for different particles at 0.2 ms ⁻¹	92
Figure 4-14d: Particle deposition (CFD) as a function of circumferential pipe angles at the up and down stream of 3 rd bend for different particles at 0.3 ms ⁻¹	92
Figure 4-14e: Particle deposition (CFD) as a function of circumferential pipe angles at the up and down stream of 3 rd bend for different particles at 0.4 ms ⁻¹	93
Figure 5-1: Flow rate and turbidity spikes in particular days for two monitoring stations (MS1 & MS2) (Prince <i>et al.</i> 2001).	100
Figure 5-2: Different arbitrary velocity and particle load profiles for the spike.	102-3
Figure 5-3: Schematic diagram of the horizontal straight pipe.	104
Figure 5-4a: Average particle distribution along the pipe at different times (0-60 minutes) for the profile of 5-2a.	106
Figure 5-4b: Average particle distribution along the pipe at different times (60-150 minutes) for the profile of 5-2a.	106
Figure 5-5a: Average particle distribution along the pipe at different times (0-60 minutes) for the profile of 5-2b.	107
Figure 5-5b: Average particle distribution along the pipe at different times (60-150 minutes) for the profile of 5-2b.	107
Figure 5-6a: Average particle distribution along the pipe at different times (0-60 minutes) for the profile of 5-2c.	108

Figure 5-6b: Average particle distribution along the pipe at different times (60-150 minutes) for the profile of 5-2c.	108
Figure 5-7a: Average particle distribution along the pipe at different times (0-60 minutes) for the profile of 5-2d.	109
Figure 5-7b: Average particle distribution along the pipe at different times (60-150 minutes) for the profile of 5-2d.	109
Figure 5-8a: Average particle distribution along the pipe at different times (0-60 minutes) for the profile of 5-2e.	110
Figure 5-8b: Average particle distribution along the pipe at different times (60-150 minutes) for the profile of 5-2e.	110
Figure 5-9a: Average particle distribution along the pipe at different times (0-60 minutes) for the profile of 5-2f.	111
Figure 5-9b: Average particle distribution along the pipe at different times (60-150 minutes) for the profile of 5-2f.	111
Figure 5-10: Average particle volume fraction as a function of time for different cross-section of pipe along length for the profile of 5-2a.	112
Figure 5-11: Average particle volume fraction as a function of time for different cross-section of pipe along length for the profile of 5-2b.	112
Figure 5-12: Average particle volume fraction as a function of time for different cross-section of pipe along length for the profile of 5-2c. .	113
Figure 5-13: Average particle volume fraction as a function of time for different cross-section of pipe along length for the profile of 5-2d.	113
Figure 5-14: Average particle volume fraction as a function of time for different cross-section of pipe along length for the profile of 5-2e.	113
Figure 5-15: Average particle volume fraction as a function of time for different cross-section of pipe along length for the profile of 2f.	114

Figure 5-16: Particle concentration at different depths along the pipe length at different time for the profile of 5-2e (a, b, and c for bottom, center, and top respectively).	115
Figure 6-1: The entrainment/deposition mechanism in a horizontal pipe.	120
Figure 6-2: The deposition flux in a tube as a function of the circumferential angle in the pipe used by Laurinat (1985).	124
Figure 6-3: Vertical cross-section of a pipe.	125
Figure 6-4: The diffusion/free-flight problem between two infinite horizontal plates.	127
Figure 6-5a: Ratio between pipe diameter and particle mean free path as a function of particle diameter at 0.1 and 0.5 ms ⁻¹ fluid velocity (D = 4310 ⁻¹ m).	133
Figure 6-5b: Ratio between pipe diameter and particle mean free path as a function of particle density at 0.1 and 0.5 ms ⁻¹ fluid velocity (D = 4.72310 ⁻¹ m).	133
Figure 6-6a: The inertial and crossing trajectories coefficients as a function of particle diameter for the velocity 0.1 and 0.5 ms ⁻¹	137
Figure 6-6b: The inertial and crossing trajectories coefficients as a function of particle specific gravity for the velocity 0.1 and 0.5 ms ⁻¹	137
Figure 6-7a: Relative concentration of particles for different height as a function of particle diameter for the velocity 0.1 ms ⁻¹	143
Figure 6-7b: Relative concentration of particles for different height as a function of specific gravity for the particle of 10 μm at velocity 0.1 ms ⁻¹	144
Figure 6-8a: Relative concentration of particles for different height as a function of particle diameter for the velocity 0.5 ms ⁻¹	144
Figure 6-8b: Relative concentration of particles for different height as a function of specific gravity for the particle of 10 μm at velocity 0.5 ms ⁻¹	144

Figure 6-9a: Comparison of the relative concentration of particles between top and bottom of the pipe as a function of the particle diameter at 0.1 and 0.5 ms ⁻¹	145
Figure 6-9b: Comparison of the relative concentration of particles between top and bottom of the pipe as a function of the particle density at 0.1 and 0.5 ms ⁻¹	146
Figure 6-10a: Deposition flux normalized by C _E (τ _p) vs circumferential pipe angle for different particle sizes (5, 10, and 20 μm) for the velocity 0.1 and 0.5 ms ⁻¹	149
Figure 6-10b: Deposition flux normalized by C _E (τ _p) vs circumferential pipe angle for different particle sizes (50, 100, and 200 μm) at 0.1 and 0.5 ms ⁻¹	149
Figure 6-10c: Deposition flux normalized by C _E (τ _p) vs circumferential pipe angle for five different particle densities (sg 1.5, 2.5, 4, 5, and 6) at 0.1 and 0.5 ms ⁻¹	149
Figure 6-11a: Comparison of analytical and simulated relative concentration as a function of particle diameter at the top of pipe at 0.1 and 0.5 ms ⁻¹	151
Figure 6-11b: Comparison of analytical and simulated relative concentration as a function of particle diameter at y = 0.75D at 0.1 and 0.5 ms ⁻¹	151
Figure 6-11c: Comparison of analytical and simulated relative concentration as a function of particle diameter at the center of pipe at 0.1 and 0.5 ms ⁻¹	151
Figure 6-11d: Comparison of analytical and simulated relative concentration as a function of particle diameter at y = 0.25D at 0.1 and 0.5 ms ⁻¹	152
Figure 6-12a: Comparison of analytical and simulated relative concentration as a function of particle weight at the top of the pipe for velocity of 0.1 and 0.5 ms ⁻¹	152

Figure 6-12b: Comparison of analytical and simulated relative concentration as a function of particle density at $y = 0.75D$ at 0.1 and 0.5 ms^{-1}	153
Figure 6-12c: Comparison of analytical and simulated relative concentration as a function of particle density weight at the center of the pipe at 0.1 and 0.5 ms^{-1}	153
Figure 6-12d: Comparison of analytical and simulated relative concentration as a function of particle density at $y = 0.25D$ at of 0.1 and 0.5 ms^{-1}	153
Figure 6-13a: Circumferential deposition as a function of circumferential pipe angles for five different particle sizes for the velocity 0.1 ms^{-1}	155
Figure 6-13b: Circumferential deposition as a function of circumferential pipe angles for five different particle sizes for the velocity 0.5 ms^{-1}	155
Figure 6-13c: Circumferential deposition as a function of circumferential pipe angles for five different particle densities for the velocity 0.1 ms^{-1}	155
Figure 6-13d: Circumferential deposition as a function of circumferential pipe angles for five different particle densities for the velocity 0.5 ms^{-1}	156

List of Tables

	Page
Table 3-1: General guidelines for flow types.....	36
Table 4-1: Physical and hydraulic characteristics of the system used for CFD simulation.....	74
Table 5-1: Physical and hydraulic characteristics of the system used for CFD simulation.....	105
Table 6-1: Properties of the different size particles with specific gravity 3.0 that are used in the Turbulent Diffusion Model.	141
Table 6-2: Properties of the different weighted particles with diameter 10 μm that are used in the Turbulent Diffusion Model.	141
Table 6-3: Properties of the fluid that are used in the Turbulent Diffusion Model.....	141
Table 6-4: Gravitational settling velocity, v_g and its ratio to free-flight velocity, v	143
Table 6-5: Physical and hydraulic characteristics of the system used for CFD simulation.	150